International Journal of Engineering Research & Technology (IJERT)
ISSN: 2278-0181
Vol. 4 Issue 05, May-2015

Vibration and Acoustic Emission Signal Monitoring for Detection of Induction Motor Bearing Fault

Mohd Sufian Othman, Mohd Zaki Nuawi
Department of Mechanical and Material Engineering
Faculty of Engineering & Built Environment
Universiti Kebangsaan Malaysia
43600 Bangi, Selangor, Malaysia

Ramizi Mohamed
Department of Electrical,
Electronic & Systems Engineering
Faculty of Engineering & Built Environment
Universiti Kebangsaan Malaysia
43600 Bangi, Selangor, Malaysia

***Abstract*— Vibration and acoustic emission (AE) signal monitoring are popular techniques for detecting bearing fault, the main cause in induction motor failure which can lead to catastrophic damage. This paper presents comparison between vibration and AE signal monitoring as a tool for induction motor bearing fault detection. The effectiveness of time-domain analysis is compared with frequency-domain. Statistical parameters used in time-domain include RMS, crest factor, and kurtosis whereas for frequency-domain, normal spectrum and envelope spectrum using Hilbert transform are applied. The results reveal that vibration and AE signals are effective measurement to detect bearing fault in both time- and frequency-domain.**

Keywords*— Induction motor bearing; fault detection; condition monitoring.

I. INTRODUCTION

Induction motor is a prominent rotating machine widely used in many industrial, commercial and domestic applications due to its efficiency, reliability, robustness, and economical. It is reported that this type of motor dominate about 96% of energy consumption for all electric motors, which consume about 40% of total electrical energy usage [1]. Although induction motor is reliable and robust, it still expose to catastrophic failure especially when running under heavy loads and long period of time. Generally, induction motor breakdown can be caused by bearing fault, shaft or coupling fault, rotor fault and stator fault [2]. Surveys revealed that bearing fault is the most typical failure in induction motor components [3], [4].

Bearing defects can be grouped as 'distributed' or 'localized' [5]–[7]. Distributed defects normally caused by manufacturing error, improper installation or abrasive wear. This group of defect include surface roughness, waviness, misaligned races, and off size ball. Whereas, localized defects are include cracks, pits, and spalls on the rolling surfaces which might be caused by fatigue failure due to overloading or shock loading of the bearings during operation and installation.

Condition monitoring is one of popular methods in determining bearing faults. Measurements such as vibration, temperature, acoustic, motor current, and wear debris are often used in bearing fault detection [8]. Among these, vibration signal is the most preferred tool in bearing fault monitoring. Fig. 1 shown typical signal condition monitoring procedure [2], [9]–[11].

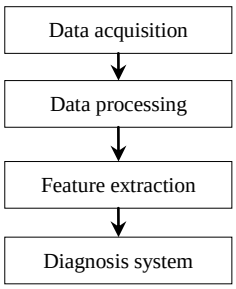

Fig. 1. Typical process for condition monitoring.

A. Time-domain Approach

Visual inspection of vibration and AE signal in time waveform is a fast method for identifying bearing damage especially for inner-race and outer-race fault. However, this method is not reliable because of noise interruption and difficulties when dealing with low amplitude signals. Statistical analysis is other basic procedure in bearing fault detection, used in past literatures considering parameters such as root mean square (RMS), crest factor, and kurtosis [12], [13].

RMS explains the effective value (magnitude) of the signal, useful to calculate the average value for variation of positive and negative values in sinusoidal signal. For N numbers of data set ($y_1, y_2, \ldots y_n$), RMS is defined as the square root of the arithmetic mean of the squares of original values ($y_1^2, y_2^2, \ldots y_n^2$) as in (1).

$$RMS = \sqrt{\frac{1}{N}\sum_{n=1}^{N} y_n^{\,2}} \qquad (1)$$

The crest factor can be defined as the ratio of the peak value to the RMS value, it yields the information about the spikiness of the measured signal. It is a pure number without any dimensions. Crest factor formula is calculated as:

$$cr = \frac{\max(|y_n|)}{RMS} \tag{2}$$

Kurtosis is the standardized 4th statistical moment of data which indicates the property of signal, whether the signal is peaked or flat relative to a Gaussian distribution. Kurtosis value is given by (3).

$$kur = \frac{\frac{1}{N}\sum_{n=1}^{N}(y_n - \mu)^4}{\sigma^4} \tag{3}$$

where μ is the mean value:

$$\mu = \frac{1}{N}\sum_{n=1}^{N}(y_n) \tag{4}$$

and σ is signal standard deviation:

$$\sigma = \sqrt{\frac{1}{N}\sum_{n=1}^{N}(y_n - \mu)^2} \tag{5}$$

B. Bearing Characteristic Frequencies

There are five characteristic frequencies exist in rotating bearing as shown in Fig. 2: (1) Shaft frequency, f_s, (2) Cage frequency, f_c, (3) Ball spin frequency, f_b, (4) Inner race frequency, f_{IR}, and (5) Outer race frequency, f_{OR} [14]–[16].

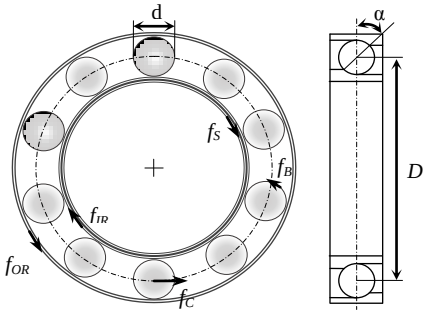

Fig. 2. Bearing dimension and characteristic frequencies.

Shaft frequency is relative speed difference between inner and outer race which can be obtained from motor rotation speed (RPM).

Cage frequency or fundamental train frequency (FTF), f_C is the rotating speed of the ball cage assembly that can be calculated as:

$$f_C = \frac{f_S}{2}\left(1 - \frac{d}{D}\cos\alpha\right) \tag{6}$$

Ball spin frequency (BSF), f_B is circular frequency of each ball as it spin which is two times the cage frequency:

$$f_B = \frac{D}{d} f_S\left(1 - \frac{d^2}{D^2}\cos^2\alpha\right) \tag{7}$$

Ball pass frequency of inner race (BPFI), f_{IR} is the frequency appeared when the ball spin across the defect in the inner race which is depend on number of balls:

$$f_{IR} = \frac{N_b f_S}{2}\left(1 - \frac{d}{D}\cos\alpha\right) \tag{8}$$

Ball pass frequency of outer race (BPFO), f_{OR} is the frequency for outer race defect:

$$f_{OR} = \frac{N_b f_S}{2}\left(1 + \frac{d}{D}\cos\alpha\right) \tag{9}$$

In these equations, N_b is the number of balls, d is the roller diameter, D is the pitch diameter of the bearing, and α is a contact angle.

In frequency-domain analysis, Fast-Fourier Transform (FFT) is an established algorithm to convert data from the time-domain. It is difficult to detect bearing fault frequencies in FFT spectrum of vibration signal [17]. However, some researchers have applied successfully [18], [19]. Furthermore, envelope spectrum using Hilbert transform can provide better result to locate fault frequencies and its resonances.

II. EXPERIMENTAL SETUP

The experimental tests were performed on test rig with a two-speed pole-changing induction motor (See Table 1). The motor is supplied by the 3 phase variable voltage transformer pre-set at 380V. Tacho generator was connected to the drive-end of motor to measure rotation speed of induction motor (Fig. 3).

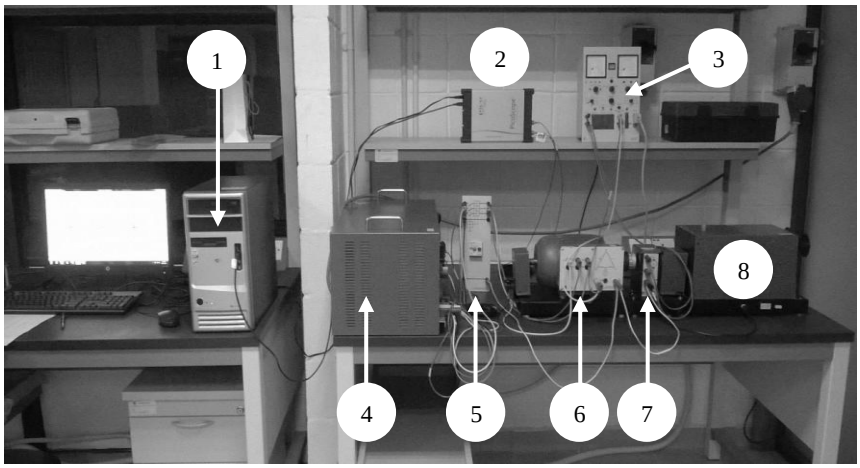

Fig. 3. Test-rig setup: (1) Computer, (2) Oscilloscope, (3) Control unit, (4) 3 Phase variable voltage supply, (5) Motor protection switch, (6) Squirrel cage induction motor, (7) Tacho generator, and (8) Magnetic powder brake.

TABLE 1. INDUCTION MOTOR SPECIFICATION

Description	Value
Make	Leybold Didactic GmbH
Model Number	732 94
Rated Power	0.7/0.95 kW
Rated Speed	1405/2825 min^{-1}
Voltage	3 Phase 380V
Frequency	50 Hz
Rated Current	2.0/2.75 A

Three bearing condition have been tested, i.e. normal bearing, bearing with inner race fault, and outer-race fault. All faulty bearings have been artificially damaged by axial drilled of ∅1mm hole through the raceways (see Fig. 4).

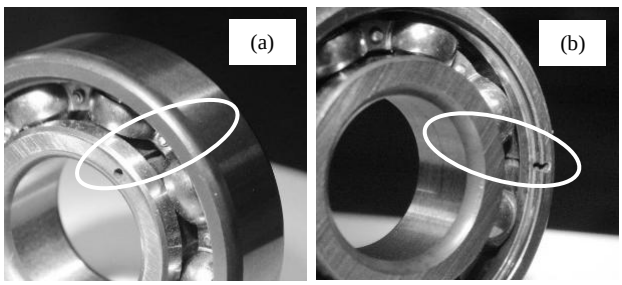

Fig. 4. Bearing with localized defect of (a) inner race and (b) outer race.

Tested bearing was placed on the drive-end of the motor. The motor then have been tested at 1450 rpm and 2900 rpm for each bearing conditions. Vibration signal is measured using SKF CMSS 9952 piezoelectric accelerometer with sensitivity of 10mV/g and the DeCI SE1000H acoustic emission transducer used to collect AE signal (Fig. 5). Data are sampled at 12 kHz using Picoscope 7000 oscilloscope.

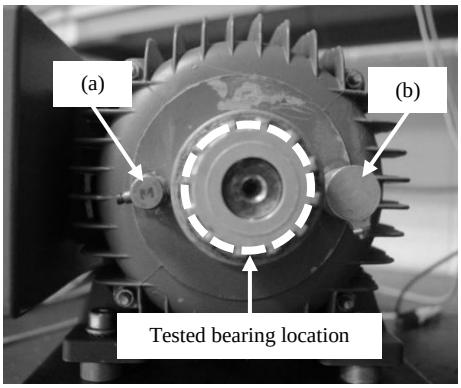

Fig. 5. *Piezoelectric accelerometer, (a) and acoustic emission transducer, (b) axially mounted on the motor casing.*

Characteristic frequencies; f_C, f_B, f_{IR}, and f_{OR} for the tested bearing are shown in Table 2, calculated based on (6), (7), (8) and (9) respectively.

TABLE 2. TESTED BEARING CHARACTERISTIC FREQUENCIES IN HERTZ

Frequency Name	1450 rpm	2900 rpm
Shaft frequency, f_S	24.17	48.33
Fundamental train frequency (FTF), f_C	9.21	18.42
Ball spin frequency (BSF) , f_B	96.26	192.51
Ball pass frequency of inner race (BPFI), f_{IR}	119.55	239.11
Ball pass frequency of outer race (BPFO), f_{OR}	73.76	147.51

III. RESULTS AND DISCUSSION

Vibration and AE signal from induction motor running without load at rotational speed of 1450 rpm and 2900 rpm have been analyzed with three methods: (1) visual inspection of time waveform, (2) statistical analysis in time-domain and (3) checking for the existence of bearing fault frequencies in normal spectrum and envelope spectrum.

A. *Time-domain Waveform Comparison*

In general, for motor rotational speed of 1450 rpm, AE signal from healthy bearing contained more values compared to acceleration signal [See Fig. 6(a)]. However, waveform for both acceleration and AE signal in 2900 rpm speed displayed in similar pattern [Refer Fig. 6(b)]. Both signals did not showed any repetitive pattern along the timeframe.

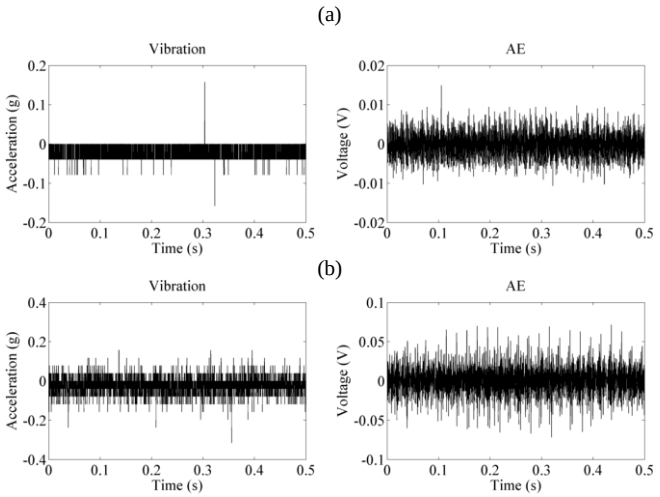

Fig. 6. Healthy bearing time waveform at (a) 1450 and (b) 2900 rpm.

Waveform of inner-race faulty bearing for 1450 rpm and 2900 rpm are presented in Fig. 7. Consistent repeating impulse is observed in vibration and AE signals for 1450 rpm, repeated at same slots. Similar pattern also observed in 2900 rpm. Although maximum peak value in vibration waveform is higher than AE signal, the quality of AE signal is better.

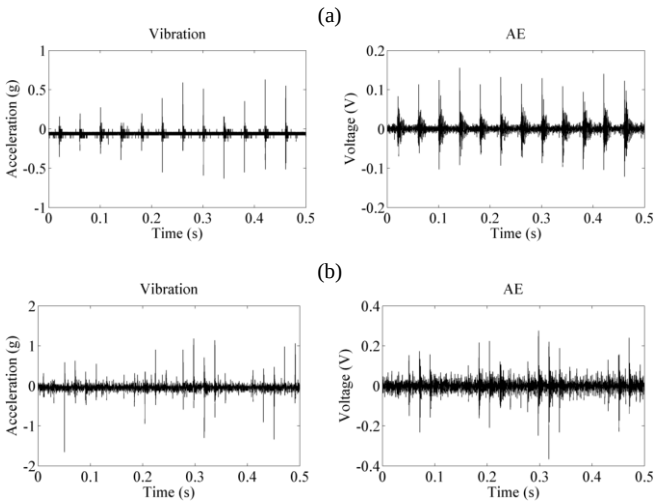

Fig. 7. Inner-race faulty bearing waveform at (a) 1450 and (b) 2900 rpm.

Fig. 8(a) and Fig. 8(b) show comparison between vibration and AE signal waveform for outer-race defected bearing in 1450 and 2900 rpm respectively. Overall shape for vibration and AE signals are about the same for both rotating speed. Repetitive peak impulse are clearly exists in small period of time compared to inner-race defected bearing.

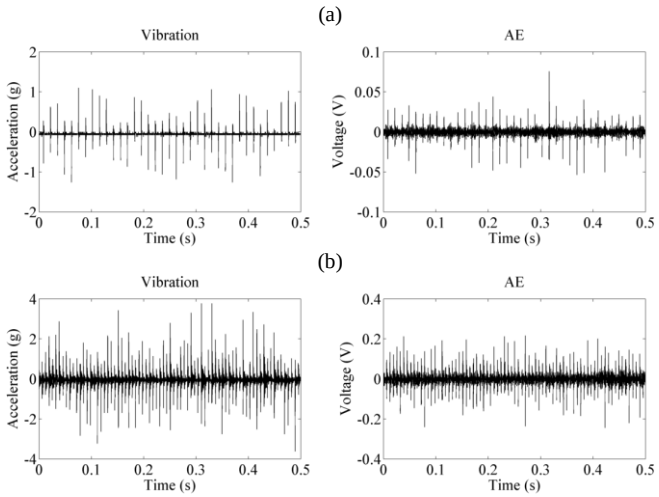

Fig. 8. Outer-race faulty bearing waveform at (a) 1450 and (b) 2900 rpm.

B. *Statistical Analysis*

Statistical values for vibration and AE signal waveform are calculated using MATLAB 8.3 for time period of 0 to 0.5 seconds, same as in time waveform analysis. Table 3 shows RMS values comparison between healthy and faulty bearing for vibration and AE signals in 1450 and 2900 rpm. RMS values for vibration signal indicate small difference between healthy and defected bearing whereas RMS values for AE signals are close to 0 in all bearing conditions. The highest RMS value is spotted in the outer-race defected bearing running at 2900 rpm.

TABLE 3. RMS VALUES COMPARISON

Bearing Condition	**Vibration**		**AE**	
	1450 rpm	***2950 rpm***	***1450 rpm***	***2950 rpm***
Healthy	0.035	0.051	0.003	0.017
Inner-race defect	0.074	0.112	0.015	0.030
Outer-race defect	0.119	0.404	0.005	0.031

Crest factor values for this experimentation data are tabulated in Table 4. There are quite large difference between crest factor values for healthy and faulty bearing for both vibration and AE signal data where the crest factor for normal bearing condition is smaller than inner-race and outer-race faulty bearing in both rotating speed.

TABLE 4. CREST FACTOR VALUE COMPARISON

Bearing Condition	Vibration		AE	
	1450 rpm	*2950 rpm*	*1450 rpm*	*2950 rpm*
Healthy	4.461	6.189	4.906	4.337
Inner-race defect	8.521	14.830	10.472	12.140
Outer-race defect	10.571	9.345	14.708	7.836

The kurtosis values for healthy and defected bearings are presented in Table 5. Generally, kurtosis value for both signal of healthy bearing is smaller than defected bearing which is close to 3, a known value for a normal distribution. The vibration signal provided higher difference between healthy and defected bearings compared to AE signal.

TABLE 5. KURTOSIS VALUES COMPARISON

Bearing Condition	Vibration		AE	
	1450 rpm	*2950 rpm*	*1450 rpm*	*2950 rpm*
Healthy	5.971	4.060	3.088	4.229
Inner-race defect	70.042	48.413	19.295	16.994
Outer-race defect	48.695	21.370	30.750	13.350

C. Envelope Spectrum Analysis

Normal spectrum and envelope spectrum analysis have been performed using normal FFT and combination of Hilbert transform with FFT respectively. Fig. 9 to Fig. 11 displayed normal spectrum whereas Fig. 12 to Fig. 14 shown envelope spectrum.

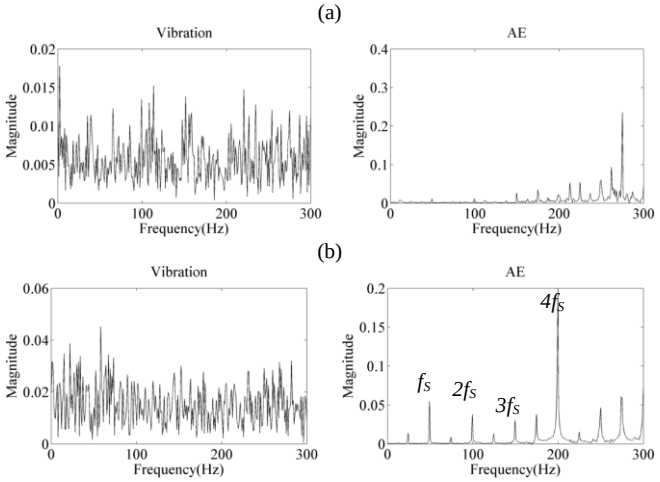

Fig. 9. Healthy bearing normal spectrum at (a) 1450 and (b) 2900 rpm.

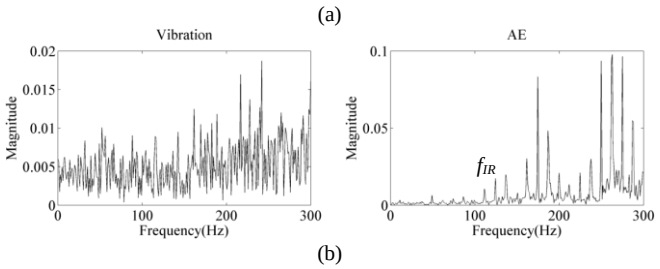

In normal FFT plot, AE spectrum is more stable than vibration spectrum. The shaft frequency, f_S is appeared only in AE spectrums at rotational speed of 2900 rpm [Refer Fig. 9(b), Fig. 10(b), and Fig. 11(b)]. Furthermore, only fault frequency of inner-race, f_{IR} is detected (Fig. 10).

After applying Hilbert transform to vibration and AE signals, the presented envelope spectrum shown more promising results. All fault frequencies appeared in both vibration and AE spectrums (Fig. 13 and Fig. 14) with clearer notification of outer-race fault frequency compared to inner-race.

Based on time-domain and frequency-domain analysis, the results reveal that vibration and AE signal monitoring are suitable procedures for detecting inner-race and outer-race bearing fault. In time waveform visual inspection, AE signal provide better information of fault occurrence. However, vibration signal provide clearer statistical parameters of RMS, crest factor, and kurtosis value to differentiate between healthy and faulty bearing. In overall comparison, RMS is the worst feature in detecting bearing fault compared to crest factor and kurtosis.

For frequency-domain analysis, normal spectrum could not locate fault frequencies except for inner-race defect. The envelope spectrum analysis using Hilbert transform is the best method suitable for detection of bearing fault frequencies in both vibration and AE envelope spectrum.

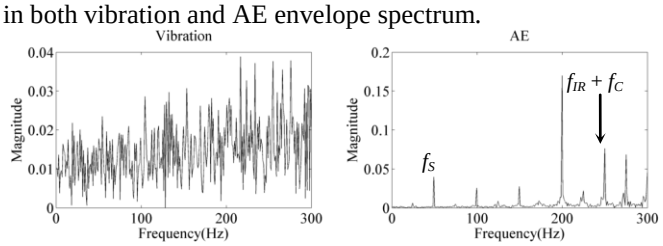

Fig. 10. Inner-race faulty bearing normal spectrum at (a) 1450 rpm and (b) 2900 rpm.

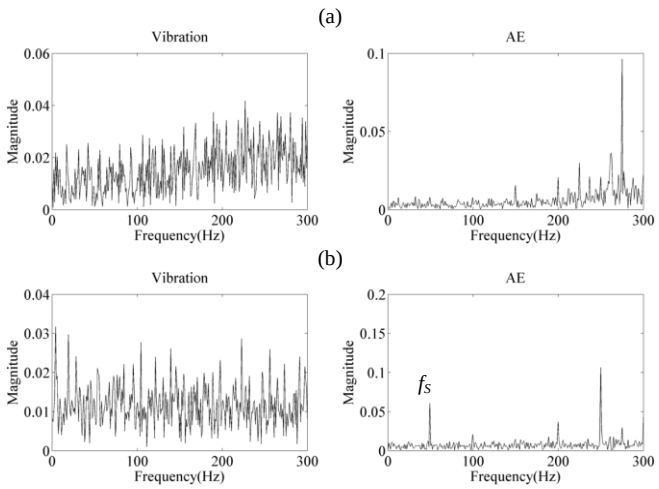

Fig. 11. Outer-race faulty bearing normal spectrum at (a) 1450 rpm and (b) 2900 rpm

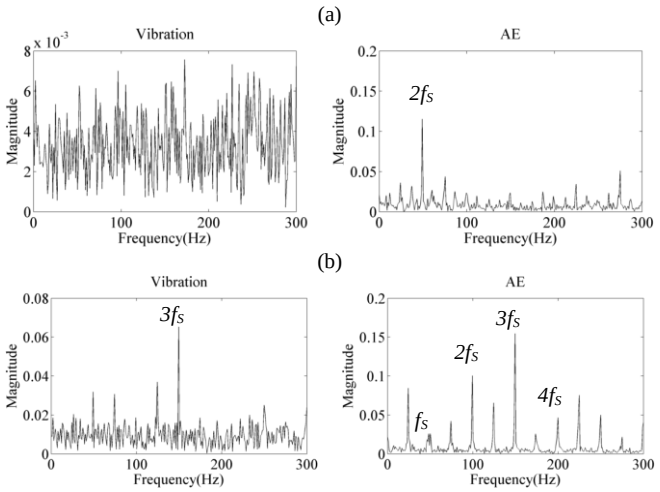

Fig. 12. Healthy bearing envelope spectrum at (a) 1450 and (b) 2900 rpm.

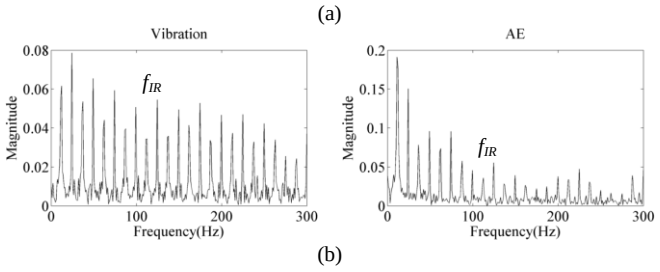

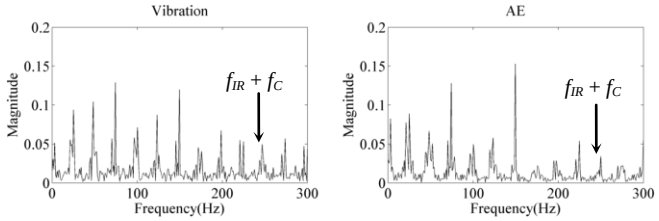

Fig. 13. Inner-race faulty bearing envelope spectrum at (a) 1450 and (b) 2900 rpm.

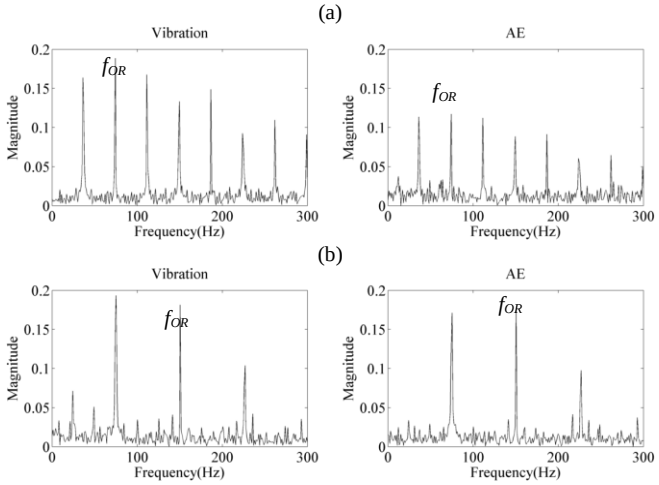

Fig. 14. Outer-race faulty bearing envelope spectrum at (a) 1450 and (b) 2900 rpm.

IV. CONCLUSION

Visual inspection of acceleration and AE signal waveform, statistical analysis and envelope spectrum monitoring are acceptable methods in detecting bearing fault. However, this procedures are time consuming and need relevant knowledge to analyze the results. Therefore, an automatic diagnosis system is essential and will be considered for future research.

REFERENCES

[1] A. T. de Almeida, F. J. T. E. Ferreira, J. Fong, and P. Fonseca, "EUP Lot 11 Motors," Coimbra, 2008.

[2] T. Han, B.-S. Yang, and Z.-J. Yin, "Feature-based fault diagnosis system of induction motors using vibration signal," *Journal of Quality in Maintenance Engineering*, vol. 13, no. 2. pp. 163–175, 2007.

[3] Motor Reliability Working Group, "Report of large motor reliability survey of industrial and commercial installations, Part 1," 1985.

[4] A. Bonnett and C. Yung, "Increased efficiency versus increased reliability," *Ind. Appl. Mag. IEEE*, vol. 1992, pp. 29–36, 2008.

[5] N. Tandon and A. Choudhury, "A review of vibration and acoustic measurement methods for the detection of defects in rolling element bearings," *Tribol. Int.*, vol. 32, no. 1999, pp. 469–480, 2000.

[6] L. Batista, B. Badri, R. Sabourin, and M. Thomas, "A classifier fusion system for bearing fault diagnosis," *Expert Syst. Appl.*, vol. 40, no. 17, pp. 6788–6797, Dec. 2013.

[7] M. D. Prieto, J. C. i Roura, J. L. R. Martínez, J. Cusidó, J. Luis, and R. Martínez, "Bearings fault detection using inference tools," in *Vibration Analysis and Control - New Trends and Developments*, F. B.- Carbajal, Ed. InTech, 2011, pp. 263–280.

[8] P. P. Kharche, "Review of Fault Detection in Rolling Element Bearing," *Int. J. Innov. Res. Adv. Eng.*, vol. 1, no. 5, pp. 169–174, 2014.

[9] V. Sugumaran and K. I. Ramachandran, "Fault diagnosis of roller bearing using fuzzy classifier and histogram features with focus on automatic rule learning," *Expert Syst. Appl.*, vol. 38, no. 5, pp. 4901–4907, 2011.

[10] H.-E. Kim, A. C. C. Tan, J. Mathew, and B.-K. Choi, "Bearing fault prognosis based on health state probability estimation," *Expert Syst. Appl.*, vol. 39, no. 5, pp. 5200–5213, Apr. 2012.

[11] B. Li, P. Zhang, Z. Wang, S. Mi, and D. Liu, "A weighted multi-scale morphological gradient filter for rolling element bearing fault detection.," *ISA Trans.*, vol. 50, no. 4, pp. 599–608, Oct. 2011.

[12] Z. Kiral and H. Karagulle, "Simulation and analysis of vibration signals generated by rolling element bearing with defects," *Tribol. Int.*, vol. 36, pp. 667–678, 2003.

[13] Y. Lei, Z. He, and Y. Zi, "Application of an intelligent classification method to mechanical fault diagnosis," *Expert Syst. Appl.*, vol. 36, no. 6, pp. 9941–9948, Aug. 2009.

[14] M. J. Devaney and L. Eren, "Detecting motor bearing faults," *IEEE Instrumentation Measurement Magazine*, vol. 7, no. 4, IEEE, pp. 30–50, 2005.

[15] J. Dybała and R. Zimroz, "Rolling bearing diagnosing method based on empirical mode decomposition of machine vibration signal," *Appl. Acoust.*, vol. 77, pp. 195–203, 2014.

[16] S. Nandi, H. A. Toliyat, and X. Li, "Condition monitoring and fault diagnosis of electrical motors - a review," *IEEE Trans. Energy Convers.*, vol. 20, no. 4, pp. 719–729, 2005.

[17] J. Zarei, "Induction motors bearing fault detection using pattern recognition techniques," *Expert Syst. Appl.*, vol. 39, no. 1, pp. 68–73, 2012.

[18] A. V Dube, L. S. Dhamande, and P. G. Kulkarni, "Vibration based condition assessment of rollingelement bearings with localized defects," *Int. J. Sci. Technol. Res.*, vol. 2, no. 4, pp. 149–155, 2013.

[19] K. Raghavendra and B. N. Karabasanagouda, "Frequency response analysis of deep groove ball bearing," *Int. J. Sci. Res.*, vol. 3, no. 8, pp. 1920–1926, 2014.